International Journal of Non-Linear Mechanics 137 (2021) 103816

Contents lists available at ScienceDirect

International Journal of Non-Linear Mechanics

journal homepage: www.elsevier.com/locate/nlm

Primary resonance of double-curved nanocomposite shells using nonlinear theory and multi-scales method: Modeling and analytical solution

Avey Mahmure [a], A.H. Sofiyev [b,*], N. Fantuzzi [c], N. Kuruoglu [d]

[a] Division of Mathematics in Graduate School of Natural and Applied Sciences of Usak University, 64000 Usak, Turkey
[b] Department of Civil Engineering of Engineering Faculty of Suleyman Demirel University, 32260 Isparta, Turkey
[c] Department of Civil, Chemical, Environmental, and Materials Engineering, University Bologna, Italy
[d] Department of Civil Engineering of Faculty of Engineering and Architecture, Istanbul Gelisim University, 34310 Avcilar/Istanbul, Turkey

ARTICLE INFO

Keywords:
Nanocomposite shells
Excitation
Primary resonance
Multi-scales method
Damping
Nonlinear forced frequency

ABSTRACT

In this article, the forced vibration of double-curved nanocomposite shells under a time dependent excitation is studied using nonlinear shell theory and multi-scales method in primary resonance. The nanocomposite representative volume element consists of two phases, including carbon nanotube (CNT) and matrix. By generalizing the Ambartsumyan's first order shear deformation shell theory (FSDT) to the heterogeneous nanocomposite shells, the nonlinear partial differential equations are derived. Then, the problem is reduced to the nonlinear forced vibration of damped nanocomposite shells with quadratic and cubic nonlinearities. For the occurrence of the primary resonance, the damping, nonlinearity, and excitation terms in the disturbance circuit are reduced to the same order. Applying the multi-scales method to nonlinear ordinary differential equation, nonlinear frequency–amplitude dependence in primary resonance is obtained.

1. Introduction

Since its inception, interest in the use of carbon nanotubes (CNTs) has attracted increasing attention due to their superior properties [1]. Modeling the superior electrical, optical, chemical, and mechanical properties of CNTs has opened new perspectives for modern technology [2]. The recent technology has eliminated some of its disadvantages related to their manipulation due to their very small size, allowing them to be used as an additive material (typical measurements of the CNT radius are in the order of 0.8–2 nm). The unique reinforcement of CNTs has allowed these materials to find potential applications in a variety of industries including textiles, medical, automotive, and mechanical engineering [3,4]. As the aerospace industry is one of the most rigorous and fundamental applications for advanced technology products, the exceptional properties of the new generation heterogeneous composites patterned by CNTs have made them one of the most attractive structural systems for this popular industry. In aerospace engineering, the use of lighter structural materials reduces the weight of aircraft, unmanned aerial vehicles and spacecraft, and balloons allow operation at higher altitudes. Unmanned vehicles have a longer operating time, faster delivery of cargo into space, long service life and low friction of CNT-reinforced composites, which allows spacecraft and similar vehicles to extend their service life [5].

The double-curved structural systems are widely used in various industries, including aircraft and rockets, shipbuilding, construction, energy, and others, and are subject to dynamic loads during exploitation. Since such elements are generally work in finite deformations, the study of their nonlinear forced vibration behavior has a long history and has never lost its relevance. A comprehensive bibliography of theoretical, numerical, and experimental studies of nonlinear vibrations of homogeneous shell-type structures in the framework of classical and shear deformation theories carried out prior to 2008 is included in the books [6–9]. Researchers have noticed over the years that one of the types of vibration that most damages mechanical systems are forced vibrations. The forced vibration can cause unpredictable damages to the structural systems in large displacements and cause structural failure. This issue has kept the investigation of forced vibration problems of shell-type members in nonlinear formulation on the agenda for many years. From the early 1980s to the 2008s, the studies on nonlinear vibration problems of homogeneous shallow shell-type systems were generally carried out using the finite element method [10–15].

The formation of a new generation of inhomogeneous composites and their use as structural members in various industries made it necessary to update their linear and non-linear forced vibration analysis. Although the number of studies on the forced vibration of such novel

* Correspondence to: Department of Civil Engineering, Suleyman Demirel University, 32260 Isparta, Turkey
E-mail addresses: mahmureavey@gmail.com (A. Mahmure), abdullahavey@sdu.edu.tr (A.H. Sofiyev), nicholas.fantuzzi@unibo.it (N. Fantuzzi), nkuruoglu@gelisim.edu.tr (N. Kuruoglu).

https://doi.org/10.1016/j.ijnonlinmec.2021.103816
Received 5 August 2021; Received in revised form 26 August 2021; Accepted 27 August 2021
Available online 2 September 2021

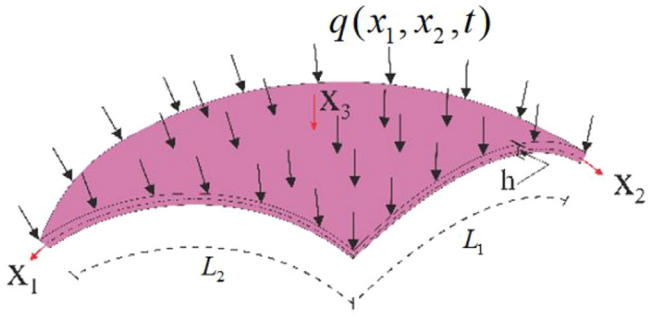

Fig. 1. Nanocomposite double-curved shell-type elements subjected to an external excitation force $q(x_1, x_2, t)$ of uncertain physical origin.

composite shell-type systems is very limited, dynamism has started to occur in studies on the subject in recent years. It is seen that most of these studies belong to nonlinear forced vibration behavior of shells composed of functionally graded isotropic materials [16–24]. The nonlinear vibration of nanocomposite members was first discussed in the study of Shen and Xiang [25], in which the nonlinear free vibration problem was formulated through mathematical modeling, and the solution was realized for the cylindrical shell patterned by CNTs. Most of the studies following this work are devoted to solving the linear and nonlinear problem of free vibrations of nanocomposite structural elements with different configurations [26,27]. The current state of vibration problems of shell-type members made of FGMs and CNT patterned materials is highlighted in the books of Shen [28], as well as in the review papers of Sofiyev [29] and Liew et al. [30].

A detailed study on the literature shows that there is only one study on nonlinear forced vibrations of double-curved nanocomposite members, and since this study deals with the thin CNT patterned shallow shell, the solution is carried out within the framework of classical shell theory [31]. As it is known, since the SDT gives more realistic results in nonlinear vibration and stability problems of moderately thick nanocomposite members, in current study, the solution of the forced vibration problem will be realized by considering the effects of transverse shear deformations. Unlike the classical shell theory, when the SDT is used, the number of basic relations and equations increases, and the solutions and numerical analyzes become more complicated. The aim of this work is to obtain analytical relations for nonlinear forced vibrations of double-curved nanocomposite shell-type members in the presence and absence of damping within SDT, as well as to study the effect of CNT patterns and volume fractions of CNT on the frequency–amplitude dependence of forced vibration considering shear strains, heterogeneity, and nonlinearity. In addition, a unique numerical analysis of the frequencies of nonlinear forced vibration of inhomogeneous nanocomposite structural members with and without damping, such as plates, panels, spherical and hyperbolic-paraboloid shells, is carried out in the framework of shear deformation and classical shell theories.

2. Setting of the problem

Fig. 1 shows a nanocomposite shallow shell with double curvature under an external excitation force $q(x_1, x_2, t)$ of uncertain physical origin. If the excitation force is assumed to be given by $q(x_1, x_2, t) = q_0 \sin(\alpha_1 x_1) \sin(\alpha_2 x_2) \cos(\varpi t)$ in which ϖ and q_0 are indicated the frequency and amplitude of external excitation, respectively [11]; $\alpha_1 = \frac{m\pi}{L_1}$ and $\alpha_2 = \frac{n\pi}{L_2}$, in which L_1 and L_2 are lengths in x_1 and x_2 directions, respectively, t is a time and (m, n) are integers corresponding to the number of vibration modes. This force is required to have finite vibration amplitude under resonance conditions. The origin of $x_1x_2x_3$ coordinate system located in the left corner of the mid-surface, the x_3 coordinate is normal to the x_1x_2 surface and is directed towards the inside of the shell. In the chosen coordinate system, the shallow shell is defined as a three-dimensional region, Λ, as follows:

$$\Lambda = \left\{x_1, x_2, x_3 : (x_1, x_2, x_3) \in [0, L_1] \times [0, L_2] \times [-0.5h, 0.5h]\right\} \tag{1}$$

where h is the thickness of shells.

The displacements are indicated by u, v and w, in the x_1, x_2, and x_3 directions respectively, the curvatures in the x_1 and x_2 directions are represented by k_1 and k_2, the radii of curvature R_1 and R_2, respectively. In this case, with $k_1 = R_1^{-1}$ and $k_2 = R_2^{-1}$, a spherical shell is defined, with $k_1 = -R_1^{-1}$ and $k_2 = R_2^{-1}$, a hypar shell is defined, with $k_1 = 0$ and $k_2 = R_2^{-1}$, a cylindrical panel is defined , and with $k_1 = k_2 = 0$ and $k_2 = R_2^{-1}$ a rectangular plate is defined (see, Fig. 2).

The mechanical properties are considered to vary smoothly through the thickness of the structure according to a predefined volume fraction due to the presence of CNTs. Such volume fraction of carbon nanotubes is considered as a linear function depending on the thickness coordinate of the nanocomposite member as [25]:

$$V_{\overline{x}_3}^{cn} = \varphi_{\overline{x}_3}^{cn} V_{cn}^*(\overline{x}_3 = x_3/h) \tag{2}$$

where V_{cnt}^* denotes the total volume fraction of carbon nanotubes and is defined as:

$$V_{cn}^* = \frac{m_{cn}}{m_{cn}\left(1 - \frac{d_{cn}}{d_m}\right) + \frac{d_{cn}}{d_m}} \tag{3}$$

m_{cn} is a mass fraction of CNTs and $\varphi_{\overline{x}_3}^{cn}$ is a linear function and is described as follows [25]:

$$\varphi_{\overline{x}_3}^{cn} = \begin{cases} 1 - 2\overline{x}_3 \\ 4\left|\overline{x}_3\right| \end{cases} \tag{4}$$

where the function $\varphi_{\overline{x}_3}^{cn} = 1 - 2\overline{x}_3$ defines the O pattern (abbreviated by OP) of CNTs in the polymer and the function $\varphi_{\overline{x}_3}^{cn} = 4\left|\overline{x}_3\right|$ defines the X pattern (abbreviated by XP) of CNTs in the polymer and the $\varphi_{\overline{x}_3}^{cn} = 1$ defines the uniform pattern (abbreviated by UP) of CNTs in the polymer.

The topology of CNT distributions determined by Eqs. (2) and (4) in the cross section of nanocomposite members is presented in Fig. 3.

The Young and shear moduli of structural systems patterned by CNTs are expressed as [25]:

$$\begin{gathered} Y_{11}(\overline{x}_3) = e_1 V_{cn}(\overline{x}_3) Y_{11}^{cn} + V^m Y^m, \frac{e_2}{Y_{22}(\overline{x}_3)} = \frac{V_{cn}(\overline{x}_3)}{Y_{22}^{cn}} + \frac{V^m}{Y^m}, \\ \frac{e_3}{S_{12}(\overline{x}_3)} = \frac{V_{cn}(\overline{x}_3)}{S_{12}^{cn}} + \frac{V^m}{S^m}, \; S_{13}(\overline{x}_3) = S_{12}(\overline{x}_3), \; S_{23}(\overline{x}_3) = 1.2 S_{12}(\overline{x}_3) \end{gathered} \tag{5}$$

where the efficiency parameters are indicated by $e_k (k = 1, 2, 3)$, the volume fraction of the polymer denotes by V_m, Young and shear moduli of the polymer (or matrix) and CNTs are denoted by Y_m, Y_{cn}^{kk} and $S_{cn}^{pk} (k = 1, 2, p = 1, 2, 3)$, respectively.

The following relation is valid for the volume fractions in the mixture: $V_{\overline{x}_3}^{cn} + V_m = 1$. Since the Poisson's ratio (P_{12}) and density (d) of nanocomposite shells are weakly dependent on the location, these mechanical properties, consisting of two components, are considered constant:

$$P_{12} = V_{cn}^* P_{11}^{cn} + V^m P^m, \;\; d = V_{cn}^* d^{cn} + V^m d^m \tag{6}$$

3. Mathematical modeling of basic relationships

According to Hooke's law, the stresses of heterogeneous nanocomposites patterned by CNTs can be associated with the strains as follows [25,28,32–34]:

$$\begin{bmatrix} \sigma_{11} \\ \sigma_{22} \\ \sigma_{12} \\ \sigma_{13} \\ \sigma_{23} \end{bmatrix} = \begin{bmatrix} Q_{11}(\overline{x}_3) & Q_{12}(\overline{x}_3) & 0 & 0 & 0 \\ Q_{21}(\overline{x}_3) & Q_{22}(\overline{x}_3) & 0 & 0 & 0 \\ 0 & 0 & Q_{66}(\overline{x}_3) & 0 & 0 \\ 0 & 0 & 0 & Q_{55}(\overline{x}_3) & 0 \\ 0 & 0 & 0 & 0 & Q_{44}(\overline{x}_3) \end{bmatrix} \begin{bmatrix} \varepsilon_{11} \\ \varepsilon_{22} \\ \gamma_{12} \\ \gamma_{13} \\ \gamma_{23} \end{bmatrix} \tag{7}$$

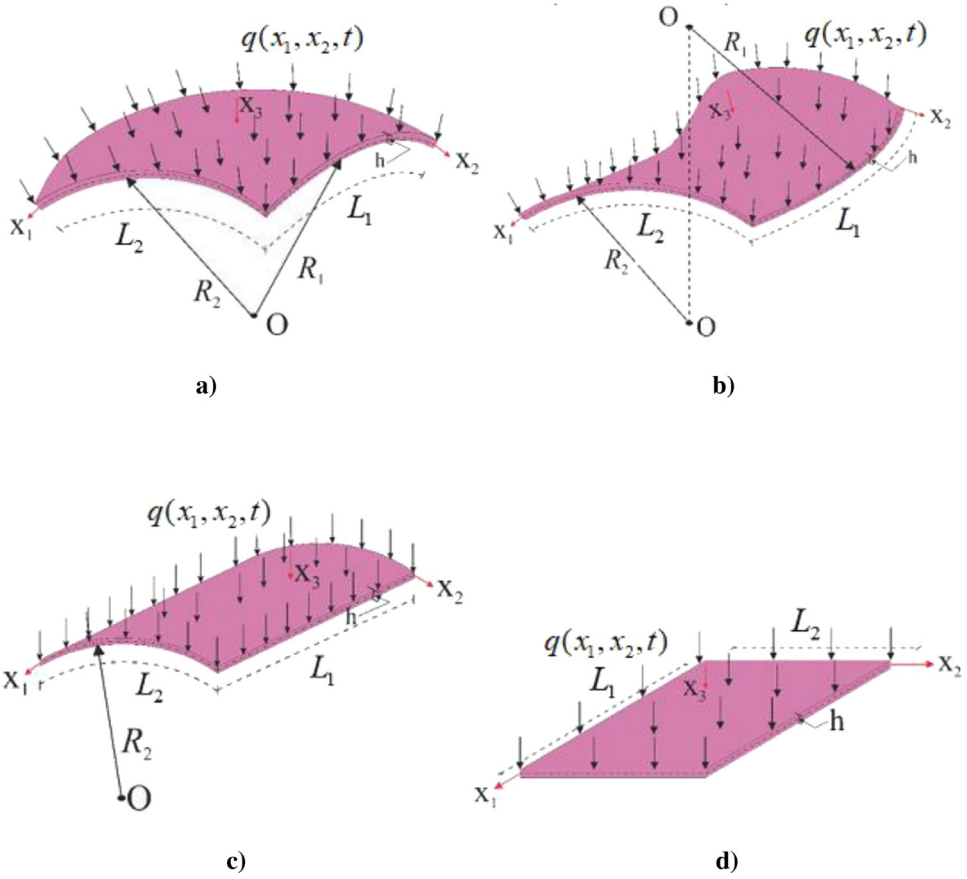

Fig. 2. Nanocomposite shell-type elements with CNT patterns under an external excitation force $q(x_1,x_2,t)$: (a) spherical shell, (b) hypar shell, (c) cylindrical panel and (d) rectangular plate.

where $Q_{ij}(\overline{x}_3),(i,j=1,2,\ldots,6)$ are stiffness coefficients of CNT patterned nanocomposites and are defined as:

$$Q_{11}(\overline{x}_3)=\frac{Y_{11}(\overline{x}_3)}{1-P_{12}P_{21}},Q_{12}(\overline{x}_3)=\frac{P_{21}Y_{11}(\overline{x}_3)}{1-P_{12}P_{21}}=\frac{P_{12}Y_{22}(\overline{x}_3)}{1-P_{12}P_{21}}=Q_{21}(\overline{x}_3),$$
$$Q_{22}(\overline{x}_3)=\frac{Y_{22}(\overline{x}_3)}{1-P_{12}P_{21}} \tag{8}$$
$$Q_{44}(\overline{x}_3)=S_{23}(\overline{x}_3),\ \ Q_{55}(\overline{x}_3)=S_{13}(\overline{x}_3),\ \ Q_{66}(\overline{x}_3)=S_{12}(\overline{x}_3)$$

The theory of anisotropic shells proposed here is based on the assumptions (Ambartsumyan [7]):

(a) The displacement $u_3=w$ normal to the middle surface of shell does not depend on the x_3 coordinate.

(b) The shear stress σ_{13} and σ_{23} or the corresponding deformations γ_{13} and γ_{23} to the thickness of the shell change according to a given law.

We point out that the first assumption, in fact, coincides with the corresponding assumption of the classical theory, and the second is a new assumption and opens up the possibility of taking into account the phenomena associated with transverse shears.

Taking hypothesis, (a) and (b), in fact, we put

$$e_{33}=0,\sigma_{13}=\frac{\mathrm{d}f}{dx_3}\phi_1(x_1,x_2,t),\ \ \sigma_{23}=\frac{\mathrm{d}f}{dx_3}\phi_2(x_1,x_2,t) \tag{9}$$

where $\phi_j(x_1,x_2,t)(j=1,2)$ are the rotations of a transverse normal to about the x_2 and x_1 axes, respectively and the shear strain function is represented by f and $\frac{\mathrm{d}f(\pm h/2)}{dx_3}=0$.

Based on the von Kármán 's kinematic nonlinearity and the assumption (9), the strain components at any point of the heterogeneous nanocomposite shells with double curvature can be expressed using the strain components on the mid-surface, changes in curvature and rotation angles as follows [6,27,31,32]:

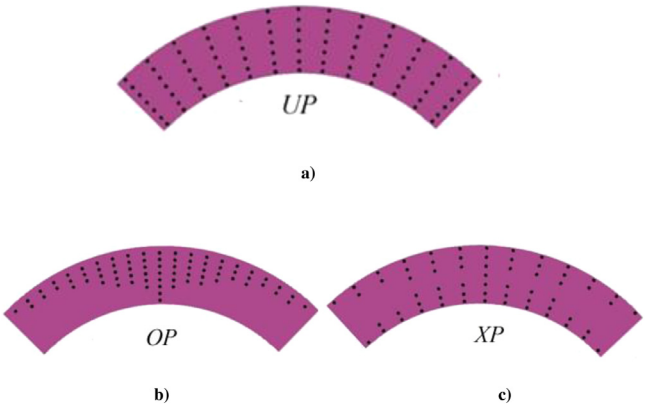

Fig. 3. Cross section of nanocomposites: (a) UP, (b) OP and (c) XP.

$$\varepsilon_{11}=\varepsilon_{11}^0-x_3\frac{\partial^2 w}{\partial x_1^2}+\Gamma_1(x_3)\frac{\partial\phi_1}{\partial x_1},\quad \varepsilon_{22}=\varepsilon_{22}^0-x_3\frac{\partial^2 w}{\partial x_2^2}+\Gamma_2(x_3)\frac{\partial\phi_2}{\partial x_2}$$
$$\gamma_{12}=\gamma_{12}^0-2x_3\frac{\partial^2 w}{\partial x_1\partial x_2}+\Gamma_1(x_3)\frac{\partial\phi_1}{\partial x_2}+\Gamma_2(x_3)\frac{\partial\phi_2}{\partial x_1} \tag{10}$$

where

$$\varepsilon_{11}^0=\frac{\partial u}{\partial x_1}-\frac{w}{R_1}+\frac{1}{2}\left(\frac{\partial w}{\partial x_1}\right)^2,\ \varepsilon_{22}^0=\frac{\partial v}{\partial x_1}-\frac{w}{R_2}+\frac{1}{2}\left(\frac{\partial w}{\partial x_2}\right)^2,$$
$$\gamma_{12}^0=\frac{\partial w}{\partial x_1}+\frac{\partial w}{\partial x_2}+\frac{\partial w}{\partial x_1}\frac{\partial w}{\partial x_2} \tag{11}$$

$$\Gamma_1(x_3)=h\int_0^{\bar{x}_3}\frac{1}{Q_{55}(\bar{x}_3)}\frac{df}{dx_3}\mathrm{d}\bar{x}_3,\quad \Gamma_2(x_3)=h\int_0^{\bar{x}_3}\frac{1}{Q_{44}(\bar{x}_3)}\frac{df}{dx_3}\mathrm{d}\bar{x}_3 \tag{12}$$

The integration of stresses across the shell thickness defines the appropriate forces (T_{ij} and N_j) and moments (M_{ij}) [6,7,9]:

$$\left(T_{ij},\ N_j\right)=h\int_{-1/2}^{1/2}\left(\sigma_{ij},\sigma_{j3}\right)\mathrm{d}\bar{x}_3,\quad M_{ij}=h^2\int_{-1/2}^{1/2}\sigma_{ij}\bar{x}_3\mathrm{d}\bar{x}_3(i,j=1,2) \tag{13}$$

Let us introduce into consideration the stress function (Φ), through which the forces are determined in the following form [6–9]:

$$T_{11}=h\frac{\partial^2\Phi}{\partial x_2^2},T_{22}=h\frac{\partial^2\Phi}{\partial x_1^2},T_{12}=-h\frac{\partial^2\Phi}{\partial x_1\partial x_2} \tag{14}$$

4. Nonlinear dynamic equations and solution

The nonlinear deformation compatibility equation of double-curved shell-type systems is derived from the literature [6] as:

$$\frac{\partial^2\varepsilon_{11}^0}{\partial x_2^2}+\frac{\partial^2\varepsilon_{22}^0}{\partial x_1^2}-\frac{\partial^2\gamma_{12}^0}{\partial x_1\partial x_2}=\left(\frac{\partial^2 w}{\partial x_1\partial x_2}\right)^2-\frac{\partial^2 w}{\partial x_1^2}\frac{\partial^2 w}{\partial x_2^2}-\left(\frac{1}{R_2}\frac{\partial^2 w}{\partial x_1^2}+\frac{1}{R_1}\frac{\partial^2 w}{\partial x_2^2}\right) \tag{15}$$

Substituting (10) into the first three relations of the system (7) and expressing deformations at the middle surface with w, Φ, ϕ_1 and ϕ_2, then substituting it into Eq. (15), the nonlinear equation of compatibility of deformations of double curved shell-type systems with CNT patterns transforms into the following view, after some operations:

$$\begin{aligned}&h\left[a_{11}\frac{\partial^4\Phi}{\partial x_2^4}+(a_{12}+a_{21}+a_{31})\frac{\partial^4\Phi}{\partial x_1^2\partial x_2^2}+a_{22}\frac{\partial^4\Phi}{\partial x_1^4}\right]\\&-a_{23}\frac{\partial^4 w}{\partial x_1^4}-\left(a_{24}+a_{13}-a_{32}\right)\frac{\partial^4 w}{\partial x_1^2\partial x_2^2}\\&-a_{14}\frac{\partial^4 w}{\partial x_2^4}+\left(\frac{1}{R_2}\frac{\partial^2 w}{\partial x_1^2}+\frac{1}{R_1}\frac{\partial^2 w}{\partial x_2^2}\right)-\left(\frac{\partial^2 w}{\partial x_1\partial x_2}\right)^2+\frac{\partial^2 w}{\partial x_1^2}\frac{\partial^2 w}{\partial x_2^2}+a_{25}\frac{\partial^3\phi_1}{\partial x_1^3}\\&+a_{15}\frac{\partial^3\phi_1}{\partial x_1\partial x_2^2}+a_{35}\frac{\partial^3\phi_1}{\partial x_1\partial x_2^2}+a_{28}\frac{\partial^3\phi_2}{\partial x_1^2\partial x_2}+a_{38}\frac{\partial^3\phi_2}{\partial x_1^2\partial x_2}+a_{18}\frac{\partial^3\phi_2}{\partial x_2^3}=0\end{aligned} \tag{16}$$

The double-curved shells with CNT patterns are subject to simply supported boundary conditions [7]:

$$\begin{aligned}&w=M_{11}=\phi_2=0,\ \text{when } x_1=0 \text{ and } L_1\\&w=M_{22}=\phi_1=0,\ \text{when } x_2=0 \text{ and } L_2\end{aligned} \tag{17}$$

Significant simplifications in theory, especially in the estimation of the nonlinear frequencies, still make the single-mode approach frequently used in the literature [6,11]. The functions w, ϕ_1, ϕ_2 that satisfy boundary conditions (17) are sought as follows:

$$\begin{aligned}&w(x_1,x_2,t)=w_0(t)\mu_{0mn}(x_1,x_2),\phi_1(x_1,x_2,t)=\phi_{10}(t)\mu_{1mn}(x_1,x_2)\\&\phi_2(x_1,x_2,t)=\phi_{20}(t)\mu_{2mn}(x_1,x_2)\end{aligned} \tag{18}$$

Here $w_0(t)$ and $\phi_{j0}(t)(j=1,2)$ are functions of the time, $\mu_{imn}(x_1,x_2),(i=0,1,2)$ are the eigenfunctions satisfying the boundary conditions (18) have the form of the Navier solution for simply supported shells as:

$$\begin{aligned}&\mu_{0mn}(x_1,x_2)=\sin(\alpha_1x_1)\sin(\alpha_2x_2),\ \mu_{1mn}(x_1,x_2)=\cos(\alpha_1x_1)\sin(\alpha_2x_2),\\&\mu_{2mn}(x_1,x_2)=\sin(\alpha_1x_1)\cos(\alpha_2x_2)\end{aligned} \tag{19}$$

Substituting approximation functions (18) to Eq. (16), the particular solution of the resulting inhomogeneous differential equation gives the following expression for Φ:

$$\Phi=k_1\cos(2\alpha_1x_1)+k_2\cos(2\alpha_2x_2)+k_3\sin(\alpha_1x_1)\sin(\alpha_2x_2) \tag{20}$$

where

$$k_1=\frac{\alpha_2^2w_0^2}{32\alpha_1^2b_{22}h},\ k_2=\frac{\alpha_1^2w_0^2}{32\alpha_2^2b_{11}h},\ k_3=\frac{\chi_1w_0+\chi_2\phi_{10}+\chi_3\phi_{20}}{h\left[b_{11}\alpha_1^4+(b_{12}+b_{21}+b_{31})\alpha_1^2\alpha_2^2+b_{22}\alpha_2^4\right]} \tag{21}$$

in which

$$\begin{aligned}&\chi_1=b_{23}\alpha_1^4+(b_{24}+b_{13}-b_{32})\alpha_1^2\alpha_2^2+b_{14}\alpha_2^4+\frac{\alpha_1^2}{R_2}+\frac{\alpha_2^2}{R_1},\\&\chi_2=-b_{25}\alpha_1^3-(b_{15}+b_{35})\alpha_1\alpha_2^2,\ \chi_3=-(b_{28}+b_{38})\alpha_1^2\alpha_2-b_{18}\alpha_2^3.\end{aligned} \tag{22}$$

Applying the Hamilton principle, the mathematical model of nonlinear dynamic equations of double-curved shell-type systems under time-dependent external excitation and viscous damping based on the SDT is generally expressed as [6]:

$$\begin{aligned}&\frac{\partial M_{11}}{\partial x_1}+\frac{\partial M_{12}}{\partial x_2}-N_1+d_1\frac{\partial^3 w}{\partial x_1\partial t^2}-d_2\frac{\partial^2\phi_1}{\partial t^2}=0\\&\frac{\partial M_{21}}{\partial x_1}+\frac{\partial M_{22}}{\partial x_2}-N_2+d_1\frac{\partial^3 w}{\partial x_2\partial t^2}-d_3\frac{\partial^2\phi_2}{\partial t^2}=0\\&\frac{\partial N_1}{\partial x_1}+\frac{\partial N_2}{\partial x_2}+\frac{T_{11}}{R_1}+\frac{T_{22}}{R_2}+T_{11}\frac{\partial^2 w}{\partial x_1^2}+2T_{12}\frac{\partial^2 w}{\partial x_1\partial x_2}+T_{22}\frac{\partial^2 w}{\partial x_2^2}+q(x_1,x_2,t)\\&=dh\frac{\partial^2 w}{\partial t^2}+2\xi dh\frac{\partial w}{\partial t}\end{aligned} \tag{23}$$

where ξ indicates the viscous damping coefficient and the parameters of rotary inertia $d_j(\mathrm{j}=1,2,3)$ are defined as:

$$d_1=d\int_{-\mathrm{h}/2}^{\mathrm{h}/2}x_3^2\mathrm{d}x_3,\ d_2=d\int_{-h/2}^{\mathrm{h}/2}x_3\Gamma_1(x_3)\mathrm{d}x_3,\ d_3=d\int_{-\mathrm{h}/2}^{\mathrm{h}/2}x_3\Gamma_2(x_3)\mathrm{d}x_3 \tag{24}$$

Considering the relationships (8), (11), (13) and (14) together in the set of Eqs. (23), the nonlinear dynamic equations of damped nanocomposite shell-type systems with double curvature are as follows:

$$\begin{aligned}&h\left[(a_{11}-a_{31})\frac{\partial^4\Phi}{\partial x_1^2\partial x_2^2}+a_{12}\frac{\partial^4\Phi}{\partial x_1^4}\right]+d_1\frac{\partial^4 w}{\partial x_1^2\partial t^2}-a_{13}\frac{\partial^4 w}{\partial x_1^4}-\left(a_{14}+a_{32}\right)\frac{\partial^4 w}{\partial x_1^2\partial x_2^2}\\&+a_{15}\frac{\partial^3\phi_1}{\partial x_1^3}+a_{35}\frac{\partial^3\phi_1}{\partial x_1\partial x_2^2}+\left(a_{18}+a_{38}\right)\frac{\partial^3\phi_2}{\partial x_1^2\partial x_2}-\Gamma_3\frac{\partial\phi_1}{\partial x_1}-d_2\frac{\partial^3\phi_1}{\partial x_1\partial t^2}=0\\&h\left[a_{21}\frac{\partial^4\Phi}{\partial x_2^4}+(a_{22}-a_{31})\frac{\partial^4\Phi}{\partial x_1^2\partial x_2^2}\right]-\left(a_{32}+a_{23}\right)\frac{\partial^4 w}{\partial x_1^2\partial x_2^2}-a_{24}\frac{\partial^4 w}{\partial x_2^4}\\&+\left(a_{35}+a_{25}\right)\frac{\partial^3\phi_1}{\partial x_1\partial x_2^2}+a_{38}\frac{\partial^3\phi_2}{\partial x_1^2\partial x_2}+a_{28}\frac{\partial^3\phi_2}{\partial x_2^3}\\&-\Gamma_4\frac{\partial\phi_2}{\partial x_2}+d_1\frac{\partial^4 w}{\partial x_1^2\partial t^2}-d_3\frac{\partial^3\phi_2}{\partial x_2\partial t^2}=0\\&h\left[-d\frac{\partial^2 w}{\partial t^2}-2\xi d\frac{\partial w}{\partial t}+\frac{1}{R_2}\frac{\partial^2\Phi}{\partial x_1^2}+\frac{1}{R_1}\frac{\partial^2\Phi}{\partial x_2^2}+\right.\\&\left.\left(\frac{\partial^2\Phi}{\partial x_2^2}\frac{\partial^2 w}{\partial x_1^2}-2\frac{\partial^2\Phi}{\partial x_1\partial x_2}\frac{\partial^2 w}{\partial x_1\partial x_2}+\frac{\partial^2\Phi}{\partial x_1^2}\frac{\partial^2 w}{\partial x_2^2}\right)\right]\\&+\Gamma_3\frac{\partial\phi_1}{\partial x_1}+\Gamma_4\frac{\partial\phi_2}{\partial x_2}+q_0\sin(\alpha_1x_1)\sin(\alpha_2x_2)\cos(\varpi t)=0\end{aligned} \tag{25}$$

where $a_{kp}(k=1,2,3,p=1,2,3,5)$ are described in Appendix A.

Applying the Galerkin procedure to the set of Eqs. (25) in the region $\Lambda_1=\left\{(x_1,x_2):0\le x_1\le L_1,0\le x_2\le L_2\right\}$, after integration, one gets:

$$\begin{aligned}&s_{11}^t\frac{\mathrm{d}^2w_0}{\mathrm{d}t^2}+s_{12}^t\frac{\mathrm{d}^2\phi_{10}}{\mathrm{d}t^2}+s_{11}w_0+s_{11}^{NL}w_0^2+s_{12}\phi_{10}+s_{13}\phi_{20}=0,\\&s_{21}^t\frac{\mathrm{d}^2w_0}{\mathrm{d}t^2}+s_{23}^t\frac{\mathrm{d}^2\phi_{20}}{\mathrm{d}t^2}+s_{21}w_0+s_{21}^{NL}w_0^2+s_{22}\phi_{10}+s_{23}\phi_{20}=0,\\&dh\frac{\mathrm{d}^2w_0}{\mathrm{d}t^2}+2\xi dh\frac{\mathrm{d}w_0}{\mathrm{d}t}+s_{31}w_0+s_{31}^{NL}w_0^2+s_{32}w_0^3\\&+s_{33}\phi_{10}+s_{34}\phi_{20}-q_0(t)\cos(\varpi t)=0\end{aligned} \tag{26}$$

where the coefficients s_{kp} $(k=1,2,3,p=1,2,3,4)$ are described in Appendix B.

Since the terms of inertia, the superscript t in the system of Eqs. (26), are ineffective due to their small value, ignoring them, excluding the functions γ_{10} and γ_{20} from the three equations, the following nonlinear ordinary differential equation CNT patterned damped structural systems with double curvature within FSDT is obtained:

$$\frac{\mathrm{d}^2 w_0}{\mathrm{d}t^2} + 2\xi\frac{\mathrm{d}w_0}{\mathrm{d}t} + \omega_{Lsdt}^2 w_0 + \lambda_1 w_0^2 + \lambda_2 w_0^3 - \lambda_3 q_0 \cos(\varpi t) = 0 \tag{27}$$

where ω_{Lsdt} denotes the linear frequency (LF) for CNT patterned structural systems with double curvature in the framework of FSDT and is defined as:

$$\omega_{Lsdt} = \left(\frac{s_{31}^*}{dh}\right)^{0.5} \tag{28}$$

and other parameters are defined as:

$$\begin{aligned}
&\lambda_1 = \frac{s_{31}^{*NL}}{dh},\quad \lambda_2 = \frac{s_{32}}{dh},\quad \lambda_3 = \frac{1}{dh},\\
&s_{31}^* = s_{31} - \frac{s_{21}s_{34}}{s_{23}} + \left(s_{33} - \frac{s_{22}s_{34}}{s_{23}}\right)\frac{s_{11}s_{23} - s_{21}s_{13}}{s_{22}s_{13} - s_{23}s_{12}}\\
&s_{31}^{*NL} = s_{31}^{NL} - \frac{s_{34}s_{21}^{NL}}{s_{23}} + \left(\frac{s_{34}s_{22}}{s_{23}} - s_{33}\right)\frac{s_{11}^{NL}s_{23} - s_{13}s_{21}^{NL}}{s_{12}s_{23} - s_{13}s_{22}}
\end{aligned} \tag{29}$$

The following initial conditions should be added to the Eq. (27) [8,9,31]:

$$w_0 = \overline{w}_0 \text{ and } \frac{\mathrm{d}w_0}{\mathrm{d}t} = 0 \text{ at } t = 0 \tag{30}$$

where $\overline{w}_0$ is the initial deflection from the equilibrium position in the center of the shells.

The occurrence of the primary resonance is required not only to satisfy the condition $\varpi \approx \omega_{Lsdt}$, but also to consider damping, nonlinearity, and excitation in the system. The existence of nonlinearity creates a term that includes $\cos(\omega_{Lsdt}t)$ for $O(\varepsilon^3)$, where ε indicates a small perturbation parameter. We need order $2\xi\frac{\mathrm{d}w_0(t)}{\mathrm{d}t}$, as $2\xi_{10}\frac{\mathrm{d}w_0(t)}{\mathrm{d}t}$, and $\lambda_3 q_0\cos(\varpi t)$, as the $\varepsilon^2\lambda_{30}\cos(\varpi t)$, so the nonlinear differential equation can be converted into:

$$\frac{\mathrm{d}^2 w_0}{\mathrm{d}t^2} + \omega_{Lsdt}^2 w_0 = -2\varepsilon^2\xi_{10}\frac{\mathrm{d}w_0}{\mathrm{d}t} - \varepsilon\lambda_{10}w_0^2(t) - \varepsilon^2\lambda_{20}w_0^3(t) + \varepsilon^2\lambda_{30}\cos(\varpi t) \tag{31}$$

where

$$\xi_{10} = \frac{\xi}{\varepsilon^2},\ \lambda_{10} = \frac{\lambda_1}{\varepsilon},\ \lambda_{20} = \frac{\lambda_2}{\varepsilon^2},\ \lambda_{30} = \frac{\lambda_3 q_0}{\varepsilon^2} \tag{32}$$

The Eq. (31) can be investigated analytically using the method of multi-scales, **a**ccording to which displacement w_0 is expanded in a series in a small parameter using new time scales in the following form [8,19]:

$$w_0(t,\varepsilon) = w_{00}(T_0,T_1,T_2) + \varepsilon w_{01}(T_0,T_1,T_2) + \varepsilon^2 w_{02}(T_0,T_1,T_2) + \cdots \tag{33}$$

where $T_n = \varepsilon^n t$ is new independent variables, among them: $T_0 = t$ is the fast time characterizing movements with natural frequencies of linear vibrations, $T_1 = \varepsilon t$ and $T_2 = \varepsilon^2 t$ are slow scales characterizing the modulation of the amplitudes and phases of nonlinear vibrations.

The expansions of the derivatives in integer order traditionally used in the multiple time scale method are as follows [8]:

$$\begin{aligned}
&\frac{\mathrm{d}}{\mathrm{d}t} = D_0 + \varepsilon D_1 + \varepsilon^2 D_2 + \cdots,\\
&\frac{\mathrm{d}^2}{\mathrm{d}t^2} = D_0^2 + 2\varepsilon D_0 D_1 + \varepsilon^2(D_1^2 + 2D_0 D_2) + \cdots
\end{aligned} \tag{34}$$

where

$$D_0 = \frac{\partial}{\partial T_0},\quad D_1 = \frac{\partial}{\partial T_1} \text{ and } D_2 = \frac{\partial}{\partial T_2} \tag{35}$$

Also since the excitation expressed as $\lambda_{30}\cos(\omega_{Lsdt}T_0 + \sigma T_2)$ in terms of T_0 and T_2 is $O(\varepsilon^2)$, for consistency the $\varpi - \omega_{Lsdt}$ is also assumed to be $O(\varepsilon^2)$ and is expressed as follows:

$$\varpi = \omega_{Lsdt} + \varepsilon^2\sigma \tag{36}$$

where σ is a parameter characterizing a small discrepancy between frequency values, i.e. the degree of their "closeness". This parameter in perturbation theory is called the "detuning parameter".

Substituting (33) and (34) into Eq. (31), after equating the coefficients with the same powers of ε to zero, we arrive at equations of various orders:

$$\varepsilon^0:\ D_0^2 w_{00} + \omega_{Lsdt}^2 w_{00} = 0 \tag{37}$$

$$\varepsilon^1:\ D_0^2 w_{01} + \omega_{Lsdt}^2 w_{01} = -2D_0D_1w_{00} - \lambda_{10}w_{00}^2 \tag{38}$$

$$\begin{aligned}
\varepsilon^2:\ &D_0^2 w_{02} + \Omega_0^2 w_{02} = -2D_0D_1w_{01} - 2D_0D_2w_{00} - D_1^2w_{00} - 2\xi_{10}D_0w_{00}\\
&-2\lambda_{10}w_{00}w_{01} - \lambda_{20}w_{00}^3 + \lambda_{30}\cos(\omega_{Lsdt}T_0 + \sigma T_2)
\end{aligned} \tag{39}$$

The solution of the second-order linear homogeneous differential equation (37) has the form:

$$w_{00} = A(T_1,T_2)e^{i\omega_{Lsdt}T_0} + \overline{A}(T_1,T_2)e^{-i\omega_{Lsdt}T_0} \tag{40}$$

where $A(T_1,T_2)$ denotes the unknown complex function and $\overline{A}(T_1,T_2)$ denotes conjugate function.

Substituting (40) into Eq. (38) one gets,

$$\begin{aligned}
D_0^2 w_{01} + \omega_0^2 w_{01} = &-2i\omega_{Lsdt}\frac{\partial A(T_1,T_2)}{\partial T_1}e^{i\omega_{Lsdt}T_0}\\
&- \lambda_{10}\left[A^2(T_1,T_2)e^{2i\omega_{Lsdt}T_0} + A(T_1,T_2)\overline{A}(T_1,T_2)\right] + CC
\end{aligned} \tag{41}$$

where CC is conjugate part to the previous terms.

In Eq. (41), to eliminate the secular terms in w_{01}, the partial derivative of $A(T_1,T_2)$ with respect to T_1 is set to zero, namely $\frac{\partial A(T_1,T_2)}{\partial T_1} = 0$ and from this equation, $A = A(T_2)$ is obtained. Therefore, the solution of Eq. (41) can be expressed as follows:

$$w_{01} = \frac{\lambda_{10}}{\omega_{Lsdt}^2}\left(-2A(T_2)\overline{A}(T_2) + \frac{1}{3}A^2(T_2)e^{2i\omega_{Lsdt}T_0} + \frac{1}{3}A^2(T_2)e^{-2i\omega_{Lsdt}T_0}\right) \tag{42}$$

Substituting expressions (40) and (42) into Eq. (39), the following secular terms from the resulting partial differential equation are set equal to zero:

$$2i\omega_{Lsdt}\left(\frac{\partial A(T_2)}{\partial T_2} + \xi_{10}A(T_2)\right) + \left(3\lambda_{20} - \frac{10\lambda_{10}^2}{3\omega_{Lsdt}^2}\right)A^2(T_2)\overline{A}(T_2) - 0.5\lambda_{30}e^{i\sigma T_2} = 0 \tag{43}$$

To solve Eq. (43), representing the functions $A(T_2)$ in the polar form, i.e., assuming that

$$A = 0.5re^{i\varphi} \tag{44}$$

where $r = r(T_2)$ and $\varphi = \varphi(T_2)$ are indicated the amplitude and phase of vibration. Then expression (44) is substituted in Eq. (43), and by separating the real and imaginary parts, the following two equations are obtained.

$$\frac{\partial r}{\partial T_2} = -\xi_{10}r + \frac{\lambda_{30}}{2\omega_{Lsdt}}\sin\psi \tag{45}$$

$$r\frac{\partial\varphi}{\partial T_2} = \frac{9\lambda_{20}\omega_{Lsdt}^2 - 10\lambda_{10}^2}{24\omega_{Lsdt}^3}r^3 - \frac{\lambda_{30}}{2\omega_{Lsdt}}\cos\psi \tag{46}$$

where ψ denotes the new phase angle that is determinant as:

$$\psi = \sigma T_2 - \varphi \tag{47}$$

Determining φ from (47) and substituting it into Eq. (46), it takes the following form:

$$r\frac{\partial\psi}{\partial T_2} = r\sigma - \frac{9\lambda_{20}\omega_{Lsdt}^2 - 10\lambda_{10}^2}{24\omega_{Lsdt}^3}r^3 + \frac{\lambda_{30}}{2\omega_{Lsdt}}\cos\psi \tag{48}$$

Steady-state motions occur for $\frac{\partial\psi}{\partial T_2} = 0$ and $\frac{\partial r}{\partial T_2} = 0$, in this case the forced vibration-amplitude relation for mechanical systems reinforced by CNTs with viscous damping for the mode (m,n) is obtained from Eqs. (45) and (48) as follows:

$$\sigma_{1,2} = \Pi h^2\bar{r}^2 \pm \left(\frac{\lambda_{30}^2}{4\omega_{Lsdt}^2 h^2\bar{r}^2} - \xi_{10}^2\right)^{0.5} \tag{49}$$

where $\bar{r} = r/h$ indicates the dimensionless vibration amplitude, and the parameter Π is expressed as follows:

$$\Pi = \frac{1}{8\omega_{Lsdt}}\left(3\lambda_{20} - \frac{10\lambda_{10}^2}{3\omega_{Lsdt}^2}\right) \tag{50}$$

In primary resonance, the nonlinear forced vibration frequency (NLFVF) for double-curved nanocomposite shell-type structures with viscous damping within SDT is expressed as:

$$\varpi_{NLsdt}^{forc_i} = \omega_{Lsdt} + \varepsilon^2\left\{\Pi h^2\bar{r}^2 \pm \left(\frac{\lambda_{30}^2}{4\omega_{Lsdt}^2 h^2\bar{r}^2} - \xi_{10}^2\right)^{0.5}\right\} \tag{51}$$

The ratio of NLFVF/LF ratio for double-curved shell-type structures patterned by CNTs can be defined by the following relationships:

$$\frac{\varpi_{NLsdt}^{forc_i}}{\omega_{Lsdt}} = 1 + \frac{\varepsilon^2}{\omega_{Lsdt}}\left\{\Pi h^2\bar{r}^2 \pm \left(\frac{\lambda_{30}^2}{4\omega_{Lsdt}^2 h^2\bar{r}^2} - \xi_{10}^2\right)^{0.5}\right\} (i = 1,2) \tag{52}$$

The expressions (51) and (52) can be used for nanocomposite spherical and hypar shells, panels and plates with and without viscous damping in the framework of FSDT, as $R_1 = R_2$, $R_1 = -R_2$, $R_1 \to \infty$ and $R_1 \to \infty$, $R_2 \to \infty$, respectively.

As $\xi = 0$, form expressions (51) and (52), NLFVF and NLFVF/LF ratio for double-curved nanocomposite elements without damping within FSDT are obtained as a special case.

As $q_0 = 0$ and $\xi = 0$, form the expression (51), the backbone curve (or ϖ_{NLsdt}^{BB}) for double-curved nanocomposite structural elements in the framework of FSDT is obtained as a special case.

When the effect of transverse shear deformations is not taken into account, the expressions (51) and (52) are valid in the framework of the classical shell theory, and CST is written instead of FSDT in the index of frequencies and their ratios.

5. Numerical applications

Applications are made using a single-mode approach to explore and validate the model created for geometrically nonlinear vibrations model of CNT patterned shells. This led both in the cases of free and forced nonlinear vibration to simple formulas, i.e., equations (51) and (52), which determine the main curves and functions of the nonlinear frequency response in terms of the nonlinear characteristics of the shells. This makes it very easy to apply the present results to different shell configurations (spherical and hypar shells, panels and plates) and different types of excitation, simply by entering into these expressions the appropriate parameter values in each case.

5.1. Validation

In Table 1, the $\varpi_{NL}^{BB}/\omega_L$ ratio for homogeneous orthotropic shells is compared with those of Sheng and Wang [18]. The ϖ_{NL}^{BB} is defined as $\varpi_{NL}^{BB} = \omega_L + \varepsilon^2\sigma_1$, in which the detuning parameter σ_1 is obtained from the expression (51) by setting $\xi_1 = 0$, $\lambda_{30} = 0$ and $V_{cn}(\bar{x}_3) = 0$.

Table 1
Comparison $\varpi_{NL}^{BB}/\omega_L$ ratio for homogeneous orthotropic shells.

r/h	Sheng and Wang [18]	Present
1.5	1.0149	1.01554
2.0	1.0265	1.02723
2.5	1.0414	1.04531

Table 2
Comparison ω_{1Lsdt} for four structural elements patterned by UP and XP in the framework of SDT.

R_1/L_1	R_2/L_2	$\omega_{1Lsdt} = \omega_{Lsdt}\left(L_1^2/h\right)\sqrt{d^m/Y^m}$				
		V_{cn}^*	Ref. [26]		Present study	
			UP	XP	UP	XP
2	2	0.11	20.238	22.432	20.286	22.493
		0.14	21.655	23.997	21.756	24.064
		0.17	25.021	27.883	25.158	27.893
2	−2	0.11	17.106	19.588	17.332	19.853
		0.14	18.626	21.225	18.924	21.512
		0.17	21.093	24.274	21.423	24.524
2	0	0.11	18.126	20.548	18.116	20.545
		0.14	19.628	22.179	19.670	22.178
		0.17	22.380	25.488	22.415	25.408
0	0	0.11	18.008	20.624	17.332	19.853
		0.14	19.608	22.349	18.924	21.512
		0.17	22.207	25.557	21.424	24.524

The initial data are used [18]: $L_2/R_2 = \pi$, $R_1 \to \infty$, $h/R_2 = 0.01$, $Y_{11}^m = 2\times10^{11}$ Pa, $Y_{22}^m = S_{12}^m = 10^{10}$ Pa, $P_{12}^m = 1/5$ and $d^m = 7.8\times10^3$ kg/m^3. When comparing the values presented in Table 1, it can be seen that our results are in good agreement with the results of [18].

In Table 2, the values of nondimensional frequency parameter $\omega_{1Lsdt} = \omega_{Lsdt}\left(L_1^2/h\right)\sqrt{d^m/Y^m}$ for spherical and hypar shells, cylindrical panels and plates with U and X patterns are compared with those of Pouresmaeeli and Fazelzadeh [26] for $(m,n) = (1,1)$, $h/L_1 = 0.05$, $L_1/L_2 = 1$. The material properties of PMMA are: $Y^m = 2.1$ GPa, $P^m = 0.34$ and $d^m = 1.15\times10^3$ kg/ m^3. The material properties of CNT is defined as follows: $Y_{11}^{cn} = 5.6466$ TPa, $Y_{22}^{cn} = 7.08$ TPa, $S_{12}^{cn} = 1.9445$ TPa, $P_{12}^{cn} = 0.175$ and $d^{cn} = 1.4\times10^3$ kg/m^3. The CNT efficiency parameters for the structural systems are used in ref. [26] as: $e_1 = 0.149, e_2 = e_3 = 0.934$ for $V_{cn}^* = 0.11$, $e_1 = 0.15, e_2 = e_3 = 0.941$ for $V_{cn}^* = 0.14$ and $e_1 = 0.149, e_2 = e_3 = 1.381$ for $V_{cn}^* = 0.17$. Looking at the results presented in Table 2, our results are in good agreement with the results in Ref. [26].

5.2. Unique numerical examples

The properties of the poly methyl methacrylate (PMMA) matrix and CNTs used in the initial numerical calculations are the same as in Table 2, only $Y^m = 2.5$ GPa is used instead of $Y^m = 2.1$ GPa. The CNT efficiency parameters for the structural systems are used as: $e_1 = 0.137, e_2 = 1.022, e_3 = 0.715$ for $V_{cn}^* = 0.12$, $e_1 = 0.142, e_2 = 1.626, e_3 = 1.138$ for $V_{cn}^* = 0.17$ and $e_1 = 0.141, e_2 = 1.585$, $e_3 = 1.109$ for $V_{cn}^* = 0.28$ [25]. The shear stress function is used as, $f = x_3(1-4x_3^2/3h^2)$. In all calculations, except Fig. 6, use the following expression for the amplitude of the external excitation [11,15,19]: $q_0 = A_q h^2 d^m \omega_L^2$. Maple software program has been used in the numerical computations.

The variations of the magnitudes of nonlinear frequencies of $\varpi_{NL}^{forc_i}$ and ϖ_{NL}^{BB} for O patterned spherical shell, hypar shell, cylindrical panel, and plate depending on the amplitude r/h for different viscous damping parameter ξ_1 in the framework of (a) SDT and (b) CST are plotted in Figs. 4a and 4b. The geometric parameters that used in numerical calculations are: $L_1/L_2 = 1, R_1/L_1 = 1, L_1/h = 20, (m,n) = (1,1)$, $V_{cn}^* = 0.12$, $A_q = 0.068$ and $\xi = \xi_1\omega_L$. Due to the increase of r/h from 0.05 to 0.61, $\varpi_{NL}^{forc_1}$ and ϖ_{NL}^{BB} frequencies of spherical and hypar shells

Table 3
Variation of $\varpi_{NL}^{forc_i}(i=1,2)$ and ϖ_{NL}^{BB} for CNT patterned spherical and hypar shells such as (a) UP and (b) OP without damping against the r/h for different V_{cn}^{*}.

		UP						OP					
		SDT			CST			SDT			CST		
V_{cn}^{*}	r/h	$\varpi_{NL}^{forc_1}$	$\varpi_{NL}^{forc_2}$	ϖ_{NL}^{BB}	$\varpi_{NL}^{forc_1}$	$\varpi_{NL}^{forc_2}$	ϖ_{NL}^{BB}	$\varpi_{NL}^{forc_1}$	$\varpi_{NL}^{forc_2}$	ϖ_{NL}^{BB}	$\varpi_{NL}^{forc_1}$	$\varpi_{NL}^{forc_2}$	ϖ_{NL}^{BB}
0.12	0.05	46.768	43.258	45.013	51.729	47.848	49.789	42.545	39.352	40.949	45.361	41.956	43.658
	0.13	45.673	44.323	44.998	50.552	49.059	49.805	41.502	40.274	40.888	44.284	42.975	43.629
	0.21	45.387	44.551	44.969	50.299	49.374	49.837	41.154	40.393	40.774	43.980	43.169	43.574
	0.29	45.229	44.624	44.926	50.217	49.548	49.883	40.881	40.330	40.605	43.787	43.200	43.493
	0.37	45.107	44.633	44.870	50.206	49.681	49.944	40.599	40.167	40.383	43.616	43.156	43.386
	0.45	44.995	44.605	44.800	50.235	49.804	50.019	40.285	39.930	40.107	43.443	43.064	43.254
	0.53	44.882	44.551	44.717	50.293	49.927	50.110	39.928	39.627	39.777	43.256	42.934	43.095
	0.61	44.763	44.476	44.620	50.374	50.056	50.215	39.524	39.263	39.394	43.050	42.771	42.910
0.17	0.05	58.057	53.745	55.901	63.244	58.546	60.895	52.928	48.996	50.962	55.778	51.634	53.706
	0.13	56.722	55.063	55.892	61.820	60.013	60.916	51.661	50.148	50.904	54.474	52.880	53.677
	0.21	56.389	55.362	55.876	61.516	60.398	60.957	51.264	50.327	50.795	54.115	53.128	53.622
	0.29	56.223	55.480	55.852	61.422	60.612	61.017	50.974	50.296	50.635	53.898	53.184	53.541
	0.37	56.111	55.528	55.820	61.414	60.779	61.096	50.689	50.158	50.424	53.714	53.154	53.434
	0.45	56.020	55.540	55.780	61.456	60.934	61.195	50.379	49.942	50.161	53.532	53.072	53.302
	0.53	55.936	55.529	55.732	61.534	61.091	61.313	50.032	49.661	49.847	53.339	52.948	53.144
	0.61	55.854	55.501	55.677	61.642	61.257	61.450	49.643	49.320	49.482	53.129	52.790	52.959
0.28	0.05	67.086	62.211	64.648	76.214	70.676	73.445	61.397	56.934	59.166	66.372	61.548	63.960
	0.13	65.540	63.664	64.602	74.532	72.402	73.467	59.902	58.185	59.043	64.830	62.974	63.902
	0.21	65.095	63.934	64.515	74.168	72.849	73.508	59.344	58.281	58.812	64.367	63.219	63.793
	0.29	64.806	63.965	64.386	74.046	73.091	73.569	58.858	58.088	58.473	64.049	63.217	63.633
	0.37	64.545	63.886	64.216	74.023	73.274	73.649	58.326	57.723	58.025	63.747	63.095	63.421
	0.45	64.276	63.734	64.005	74.056	73.440	73.748	57.716	57.220	57.468	63.426	62.890	63.158
	0.53	63.982	63.522	63.752	74.128	73.605	73.866	57.013	56.592	56.802	63.071	62.616	62.844
	0.61	63.658	63.259	63.459	74.231	73.778	74.004	56.211	55.845	56.028	62.676	62.281	62.478

with and without damping decrease, while the $\varpi_{NL}^{forc_2}$ first increases, and after reaching the maximum value, it decreases in the framework of FSDT and CST. The $\varpi_{NL}^{forc_2}$ and ϖ_{NL}^{BB} for the cylindrical panel and plate increase, while the $\varpi_{NL}^{forc_1}$ decreases due to increase of the r/h. In addition, for all structural elements $\varpi_{NL}^{forc_2}$ increases, while $\varpi_{NL}^{forc_1}$ reduces, as the viscous damping parameter ξ_1 increases from 0 to 0.09. The effect of viscous damping on the nonlinear frequencies for all considered structural elements increases with increasing of r/h. For example, depending on the increase of r/h from 0.05 to 0.53, the influences of viscous damping on the nonlinear forced vibration frequencies are increased by (4.4%), (6%), (3.8%) and (3.7%) for the spherical shell, hypar shell, cylindrical panel and plate, respectively with a fixed $\xi_1 (= 0.07)$. The viscous damping effects on $\varpi_{NL}^{forc_1}$ and $\varpi_{NL}^{forc_1}$ for spherical and hypar shells, panel and plate with the O pattern increase by (4.8%) and (6%), (5.8%) and (7.66%), (4.53%) and (5.51%), and (4.46%) and (5.41%), respectively, as the ξ_1 increases from 0.03 to 0.09 for fixed r/h (=0.33) within SDT, whereas those effects are around (1%) smaller within CST. The effect of shear strains on $\varpi_{NL}^{forc_1}$ increases weakly, while on $\varpi_{NL}^{forc_2}$ for spherical and hypar shells it decreases weakly, but vice versa for the panel and plate, as ξ_1 increases.

Table 3 shows the variation of $\varpi_{NL}^{forc_i}(i=1,2)$ and ϖ_{NL}^{BB} for two different patterned (a) spherical and (b) hypar shells such as UP and OP without damping against r/h for $V_{cn}^{*}=0.12$, 0.17, 0.28 within FSDT and CST. The dashed curves correspond to the nonlinear backbone frequency, ϖ_{NL}^{BB}. The following parameters are used in drawing the curves: $R_1/L_1=2$, $L_1/L_2=1$, $L_1/h=20$, $A_q=0.004$ and $(m,n)=(1,1)$. The effects of shear strains on $\varpi_{NLsdt}^{forc_i}(i=1,2)$ and ϖ_{NL}^{BB} for both shallow shells increase due to the increase of r/h. For instance, depending on the increase of r/h from 0.05 to 0.61, the influences of shear strains on $\varpi_{NLsdt}^{forc_i}(i=1,2)$ and ϖ_{NL}^{BB} for the spherical shell increase from (11.98%) to (14.26%) and from (7.49%) to (10.33%), while those effects in the hypar shells increase from (13.79%) to (16.41%) and from (9.14%) to (13.15%) for U and O patterns, respectively, at $V_{cn}^{*}=0.28$. The effects of shear strains on $\varpi_{NLsdt}^{forc_i}(i=1,2)$ and ϖ_{NL}^{BB} for spherical shells with the O pattern are (8.2%), (6.57%), and (10.33%), whereas those effects for hypar shells are (10.59%), (8.66%), and (13.15%), respectively for $V_{cn}^{*}=0.12$, 0.17 and 0.28. As can be seen, the V_{cn}^{*} effect on frequencies is more pronounced in hypar shells. Additionally, the greatest shear strains effects occur at $V_{cn}^{*}=0.28$ in the hypar shallow shells, while the smallest effects occur at $V_{cn}^{*}=0.17$ in the shallow spherical shell. The effect of the O pattern on the $\varpi_{NLsdt}^{forc_i}(i=1,2)$ and ϖ_{NL}^{BB} for both shallow shells increase due to the increase of r/h. In addition, the largest O pattern effect differences between $V_{cn}^{*}=0.12$ and $V_{cn}^{*}=0.17$, and between $V_{cn}^{*}=0.12$ and $V_{cn}^{*}=0.28$ in the spherical shell are (0.6%) and (0.55%), whereas this difference in the hypar shell are (0.46%) and (0.44%), respectively, at $r/h=0.61$.

The changes of $\varpi_{NLsdt}^{forc_i}(i=1,2)$ and ϖ_{NL}^{BB} for two different CNT patterned (a) spherical and (b) hypar shells without damping depending on the r/h for different excitation amplitude, q_0 in the framework of SDT and CST are illustrated in Fig. 5. This analysis takes into account U and O patterned shells, and uses the following geometrical data related to them: $V_{cn}^{*}=0.12$, $q_0=\{0.1,0.3,0.5\}\times10^5$ (Pa), $R_1/L_1=3$, $L_1/h=20$, $L_1/L_2=1$, $(m,n)=(1,1)$. Due to the increase of q_0, the $\varpi_{NL}^{forc_1}$ of shallow shells increase and the $\varpi_{NL}^{forc_2}$ decrease, while the $\varpi_{NL}^{forc_i}(i=1,2)$ and ϖ_{NL}^{BB} for the spherical shell are more pronounced than those of the hypar shell. When the difference between the $\varpi_{NL}^{forc_1}$ for the shallow shells is examined, it is observed that the difference between the $\varpi_{NL}^{forc_2}$ increases while this difference decreases due to the increase of q_0 from 0.1×10^5 to 0.5×10^5 (Pa).

The effect of shear strains on $\varpi_{NL}^{forc_1}$ for shallow shells decreases due to the increase of q_0, while this effect on the $\varpi_{NL}^{forc_2}$ increases. For instance, due to the rise of q_0 from 0.1×10^5 to 0.5×10^5 (Pa) for $r/h=0.05$, the shear strains effect on the $\varpi_{NL}^{forc_1}$ for the spherical shell patterned by OP decreases from (7.04%) to (5.80%), it increases from (7.76%) to (9.41%) for $\varpi_{NL}^{forc_2}$. Likewise, the shear strains effect on the $\varpi_{NL}^{forc_1}$ for the hypar shell with the OP decreases from (8.24%) to (6.55%), while it increases from (9.22%) to (11.55%) for $\varpi_{NL}^{forc_2}$. The influence of shear strains on the $\varpi_{NL}^{forc_i}(i=1,2)$ of the spherical shell is smaller than its effect on the frequencies of the hypar shell. The shear strains effect difference between shallow shells patterned by UP decreases (0.3%) and (1.36%) for $\varpi_{NL}^{forc_1}$ and $\varpi_{NL}^{forc_2}$, respectively due to the increase of r/h from 0.05 to 0.61, at $q_0=0.5\times10^5$. Depending

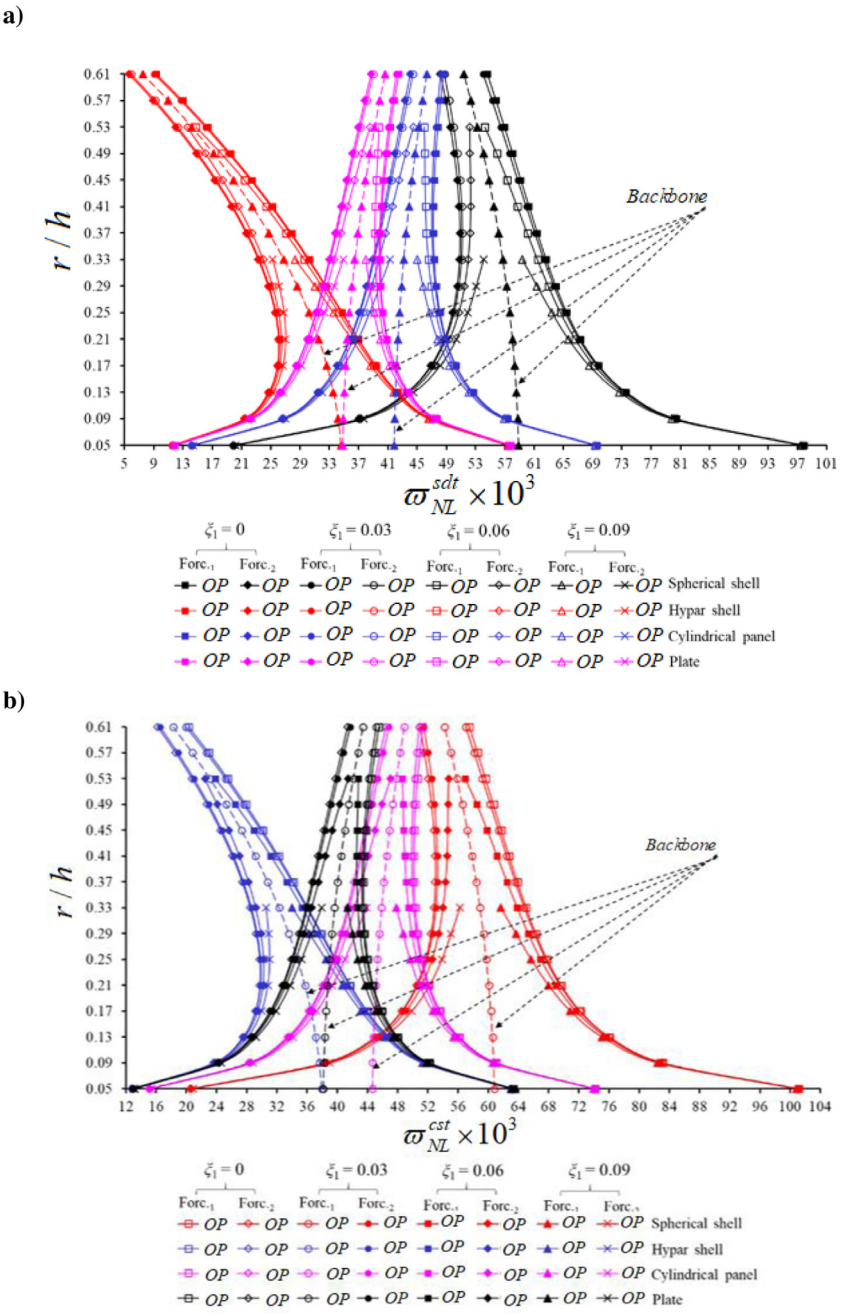

Fig. 4. Variation of magnitudes of $\varpi_{NL}^{forc_i}(i=1,2)$ and ϖ_{NL}^{BB} for O patterned structural systems against the r/h for different damping parameter ξ_1 within SDT and CST.

on the increase of q_0 from 0.1×10^5 to 0.5×10^5(Pa), while shear strains effect difference between shallow shells patterned with OP decreases for $\varpi_{NL}^{forc_1}$ by (0.44%), it increases (0.68%) for $\varpi_{NL}^{forc_2}$, at $r/h=0.61$.

Due to the increase of r/h from 0.05 to 0.61 and when $q_0 = 0.5\times10^5$(Pa), the OP effect on the $\varpi_{NL}^{forc_1}$ and ϖ_{NL}^{BB} for the spherical shell within SDT increases (3.4%) and (1.3%) respectively, it reduces first by (2.1%) and then increases by (0.77%) for $\varpi_{NL}^{forc_2}$. Similarly, due to the rise in r/h from 0.05 to 0.61, the influence of the OP on the $\varpi_{NL}^{forc_1}$ and ϖ_{NL}^{BB} for the spherical shell in the framework of CST increases (2.96%) and (0.71%), respectively, it decreases first by (2.3%) and then slightly increases by (0.3%) for $\varpi_{NL}^{forc_2}$. Depending on the increase of r/h from 0.05 to 0.61 when $q_0 = 0.5\times10^5$, the O pattern effect on the $\varpi_{NL}^{forc_1}$ and ϖ_{NL}^{BB} for the hypar shell within SDT increases (3.1%) and (0.43%), respectively, it reduces first by (3.13%) and then slightly increases by (0.1%) for $\varpi_{NL}^{forc_2}$. Likewise, depending on the rise in r/h amplitude from 0.05 to 0.61, the influence of the O pattern on the $\varpi_{NL}^{forc_2}$ and ϖ_{NL}^{BB} of the spherical shell in the framework of CST reduces (1.35%) and (0.3%) respectively, it increases first by (0.7%) and then slightly decreases by (0.1%) for $\varpi_{NL}^{forc_1}$.

Due to the increase of q_0 from 0.1×10^5 to 0.5×10^5(Pa) at $r/h=0.05$, the O pattern effect on the $\varpi_{NL}^{forc_1}$ of the spherical shell reduces (1.81%) and (1.94%) for SDT and CST, respectively, while the effect of the OP on $\varpi_{NL}^{forc_2}$ of the spherical shell increases (2.34%) and (2.38%) for SDT and CST, respectively. Likewise, the OP effect on the $\varpi_{NL}^{forc_1}$ for the hypar shell reduces (2.26%) and (2.34%) within SDT and CST, respectively, while the influence of OP on the $\varpi_{NL}^{forc_2}$ for the hypar shell increases (3.05%) and (2.95%) within SDT and CST, respectively.

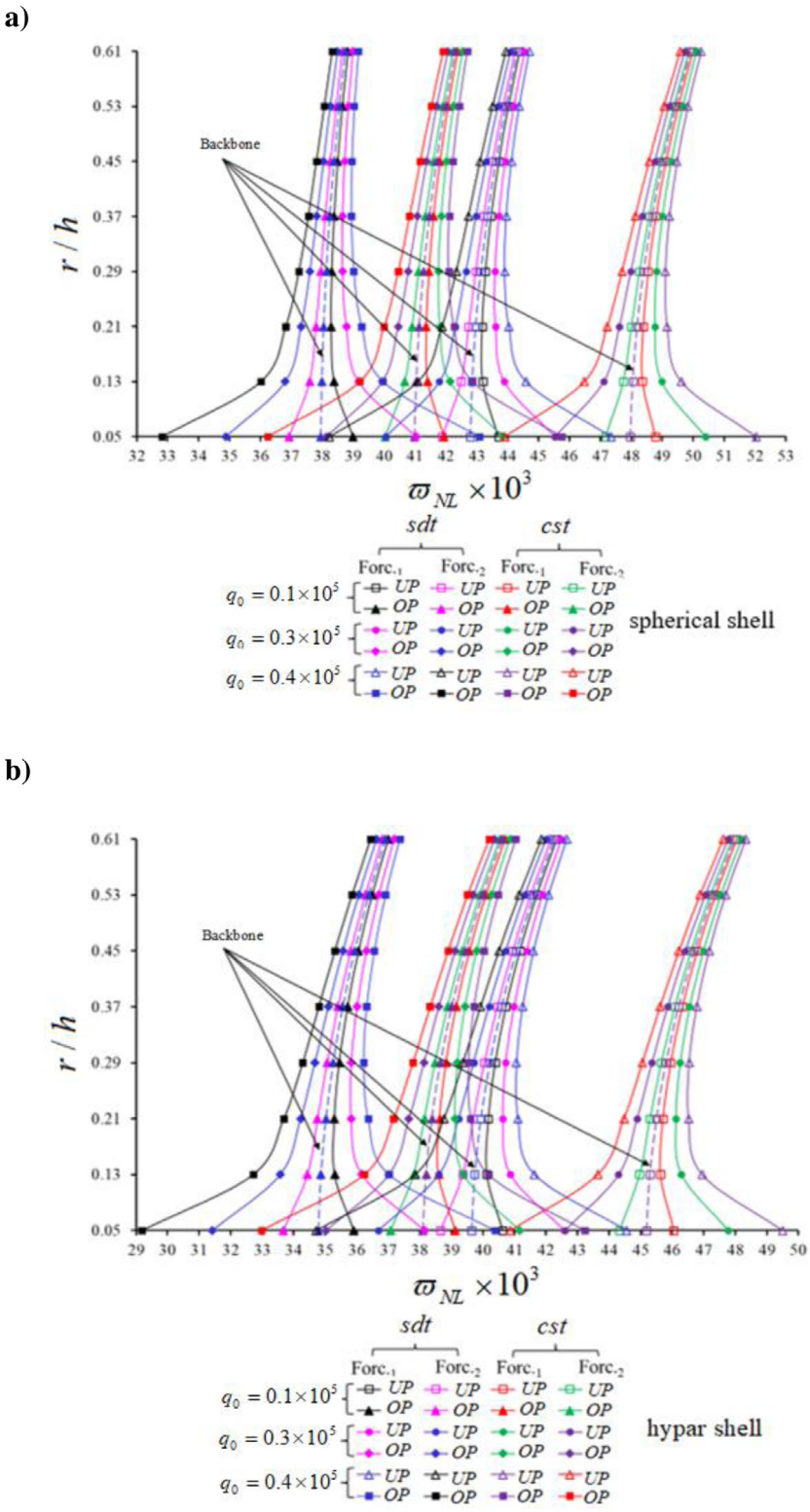

Fig. 5. Variation of $\varpi_{NL}^{forc_i}(i=1,2)$ and ϖ_{NL}^{BB} for CNT patterned (a) spherical and (b) hypar shells the r/h for different excitation amplitude q_0 within SDT and CST.

The changes of nonlinear forced vibration frequency to linear frequency ratios of two different CNT patterned (a) spherical and (b) hypar shells without damping against the amplitude r/h in the framework of SDT with different R_1/L_1 are shown in Fig. 6. This analysis takes into account U and X patterned shells, and uses the following geometrical data related to them: $V_{cn}^* = 0.12$, $R_1/L_1 = 1.0, 1.5, 2.0$, $L_1/h = 20$, $L_1/L_2 = 0.5$, $A_q = 0.004$ and $(m,n) = (1,1)$. While the $\varpi_{NLsdt}^{forc_1}/\omega_{Lsdt}$ and $\varpi_{NLsdt}^{BB}/\omega_{Lsdt}$ ratios of the spherical shell patterned by UP decrease due to the increase of r/h from 0.05 to 0.61, $\varpi_{NLsdt}^{forc_2}/\omega_{Lsdt}$ ratio first increases and becomes a maximum and then decreases for all R_1/L_1. While $\varpi_{NLsdt}^{forc_1}/\omega_{Lsdt}$ and $\varpi_{NLsdt}^{BB}/\omega_{Lsdt}$ ratios of the hypar shell patterned by UP decrease due to the rise of r/h

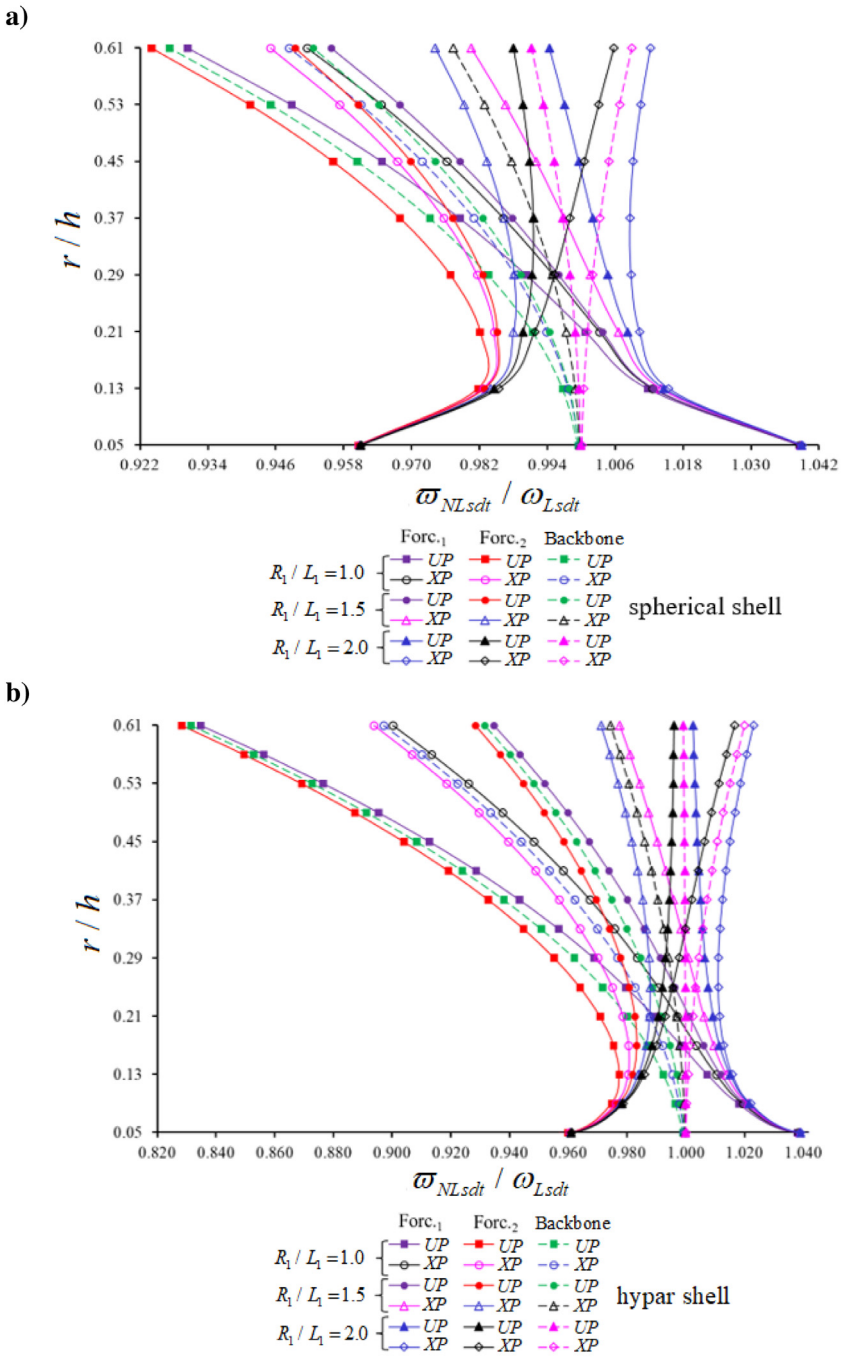

Fig. 6. Variation of $\varpi^{forc_i}_{NLsdt}/\omega_{Lsdt}$ for two different CNT patterned (a) spherical and (b) hypar shells on the r/h in the framework of SDT with different R_1/L_1.

in the range of $R_1/L_1 < 2$, $\varpi^{forc_2}_{NLsdt}/\omega_{Lsdt}$ ratio first increases and becomes a maximum and then decreases. Depending on the increase of r/h, when $R_1/L_1 = 2$, the $\varpi^{forc_1}_{NLsdt}/\omega_{Lsdt}$ and $\varpi^{BB}_{NLsdt}/\omega_{Lsdt}$ ratios of the hypar shell patterned by UP decrease, while $\varpi^{forc_2}_{NLsdt}/\omega_{Lsdt}$ ratios increase. Depending on the rise of r/h in the range of $R_1/L_1 < 2$, while $\varpi^{forc_1}_{NLsdt}/\omega_{Lsdt}$ and $\varpi^{BB}_{NLsdt}/\omega_{Lsdt}$ ratios of shallow shells patterned with XP decrease, $\varpi^{forc_2}_{NLsdt}/\omega_{Lsdt}$ ratios first increase and become maximum and then decrease. When $R_1/L_1 = 2$, $\varpi^{forc_2}_{NLsdt}/\omega_{Lsdt}$ and $\varpi^{BB}_{NLsdt}/\omega_{Lsdt}$ ratios of shallow shells patterned by XP increase due to the increase of r/h, while $\varpi^{forc_1}_{NLsdt}/\omega_{Lsdt}$ ratios first decrease and become minimum and then increase. Besides, the frequency ratios of shallow shells increase with the increase of the R_1/L_1 ratio from 1 to 2. Due to the increase of r/h from 0.05 to 0.61 at $R_1/L_1 = 2$, the effect of the XP on the frequency ratios increases (2.27%) and (7.87%) for the spherical and hypar shells, respectively. Depending on the increase of R_1/L_1 from 1 to 2, while the effect of the XP on the frequency ratios of the hypar shell increases, this effect on the frequency ratios of the spherical shell first increases and then reduces. For instance, due to the rise of R_1/L_1 ratio from 1 to 2 at $r/h = 0.61$, the influence of X pattern on frequency ratios decreases in the hypar shell by (5.84%), while it first slightly increases

by (0.33%) and then slightly decreases by (0.8%) in the spherical shell. The XP effect on the frequency ratios of hypar shells is greater than the effect on the spherical shell. While the largest XP difference between spherical and hypar shells occurs at $R_1/L_1 = 1$ and $r/h = 0.61$, it decreases by (5.6%) due to the increase of R_1/L_1 from 1 to 2.

6. Conclusions

The forced vibration of CNT patterned double-curved nanocomposite shells with and without viscous damping is investigated within nonlinear shell theories. After mathematically modeling double-curved structural systems with CNT patterns, the nonlinear fundamental differential equations have been derived in the framework of FSDT. Then, using the Galerkin method, the problem is reduced to the NLFV of continuous systems patterned by CNTs in the absence of viscous damping with quadratic and cubic nonlinearities. By applying the method of multiple scales to the ordinary differential equation with quadratic and cubic nonlinearities, the nonlinear forced frequency–amplitude relation with viscous damping and relation of the backbone curve are obtained.

Numerical analysis reveals the following generalized results:

(a) Due to the increase of r/h, $\varpi_{NL}^{forc_1}$ and ϖ_{NL}^{BB} frequencies of spherical and hypar shells with and without damping decrease, while the $\varpi_{NL}^{forc_2}$ first increases, and after reaching the maximum value, it decreases in the framework of SDT and CST.
(b) The $\varpi_{NL}^{forc_2}$ and ϖ_{NL}^{BB} for the cylindrical panel and plate increase, while the $\varpi_{NL}^{forc_1}$ decreases due to increase of the r/h.
(c) For all structural elements $\varpi_{NL}^{forc_2}$ increases, while $\varpi_{NL}^{forc_1}$ reduces, as the viscous damping parameter ξ_1 increases.
(d) The effect of viscous damping on the nonlinear frequencies for all considered structural elements increases with increasing of r/h.
(e) The effect of shear strains on $\varpi_{NL}^{forc_1}$ increases weakly, while on $\varpi_{NL}^{forc_2}$ for spherical and hypar shells it decreases weakly, but vice versa for the panel and plate, as ξ_1 increases.
(f) Depending on the increase of q_0, while shear strains effect difference between shallow shells patterned with OP decreases for $\varpi_{NL}^{forc_1}$, it increases for $\varpi_{NL}^{forc_2}$, at $r/h = 0.61$.
(g) Due to the increase of q_0, the $\varpi_{NL}^{forc_1}$ of shallow shells increase and the $\varpi_{NL}^{forc_2}$ decrease, while the $\varpi_{NL}^{forc_i}(i = 1, 2)$ and ϖ_{NL}^{BB} for the spherical shell are more pronounced than those of the hypar shell.
(h) The effect of shear strains on $\varpi_{NL}^{forc_1}$ for shallow shells decreases due to the increase of q_0, while this effect on the $\varpi_{NL}^{forc_2}$ increases.
(i) The greatest shear strains effects on the $\varpi_{NLsdt}^{forc_i}(i = 1, 2)$ and ϖ_{NL}^{BB} occur at $V_{cn}^* = 0.28$ in the hypar shallow shells, while the smallest effects occur at $V_{cn}^* = 0.17$ in the shallow spherical shell.
(j) The effect of the O pattern on the $\varpi_{NLsdt}^{forc_i}(i = 1, 2)$ and ϖ_{NL}^{BB} for both shallow shells increase due to the increase of r/h.
(k) The largest O pattern effect differences between $V_{cn}^* = 0.12$ and $V_{cn}^* = 0.17$, and between $V_{cn}^* = 0.12$ and $V_{cn}^* = 0.28$ occur in the spherical shell.
(l) The influence of shear strains on the $\varpi_{NL}^{forc_i}(i = 1, 2)$ of the spherical shell is smaller than its effect on the frequencies of the hypar shell.

CRediT authorship contribution statement

Avey Mahmure: Conceptualization, Formal analysis, Investigation, Writing - original draft. **A.H. Sofiyev:** Methodology, Writing - review & editing. **N. Fantuzzi:** Formal analysis, Writing - review & editing. **N. Kuruoglu:** Writing - review & editing.

Declaration of competing interest

The authors declare that they have no known competing financial interests or personal relationships that could have appeared to influence the work reported in this paper.

Author statement

We confirm that, this is an original paper, has not been submitted elsewhere for publication and has not been published elsewhere.

Funding source

This article has no funding support.

Appendix A

$a_{kp}, b_{kp}(k = 1, 2, 3, p = 1, 2, \dots, 8)$ and $\Gamma_k(k = 3, 4)$ are defined as,

$$
\begin{aligned}
&a_{11} = c_{111}b_{11} + c_{121}b_{21},\ a_{12} = c_{111}b_{12} + c_{121}b_{11},\\
&a_{13} = c_{111}b_{13} + c_{121}b_{23} + c_{112},\\
&a_{14} = c_{111}b_{14} + c_{121}b_{24} + c_{122},\ a_{15} = c_{111}b_{15} + c_{121}b_{25} + c_{151},\\
&a_{18} = c_{111}b_{18} + c_{121}b_{28} + c_{181},\\
&a_{21} = c_{211}b_{11} + c_{221}b_{21},\ \ a_{22} = c_{211}b_{12} + c_{221}b_{22},\\
&a_{23} = c_{211}b_{13} + c_{221}b_{23} + c_{212},\\
&a_{24} = c_{211}b_{14} + c_{221}b_{24} + c_{222},\ a_{25} = c_{211}b_{15} + c_{221}b_{25} + c_{251},\\
&a_{28} = c_{211}b_{18} + c_{221}b_{28} + c_{281},\\
&a_{31} = c_{661}b_{35},\ \ a_{32} = c_{661}b_{32} + 2c_{662},\ \ a_{35} = c_{351} - c_{661}b_{35},\\
&a_{38} = c_{381} - c_{661}b_{38},\\
&\Gamma_k = \int_{-h/2}^{h/2} \frac{df}{dx_3}\mathrm{d}x_3, (k = 3, 4)
\end{aligned}
\tag{A.1}
$$

where

$$
\begin{aligned}
&b_{11} = \frac{c_{220}}{\Delta},\ \ b_{12} = -\frac{c_{120}}{\Delta},\ \ b_{13} = \frac{c_{120}c_{211} - c_{111}c_{220}}{\Delta},\ \ b_{14} = \frac{c_{120}c_{211} - c_{121}c_{220}}{\Delta},\\
&b_{15} = \frac{c_{250}c_{120} - c_{150}c_{220}}{\Delta}, b_{18} = \frac{c_{280}c_{120} - c_{180}c_{220}}{\Delta},\ \ b_{21} = -\frac{c_{210}}{\Delta},\ \ b_{22} = \frac{c_{110}}{\Delta},\\
&b_{23} = \frac{c_{111}c_{210} - c_{211}c_{110}}{\Delta},\ \ b_{24} = \frac{c_{121}c_{210} - c_{221}c_{110}}{\Delta},\ \ b_{25} = \frac{c_{150}c_{210} - c_{250}c_{110}}{\Delta},\\
&b_{31} = \frac{1}{c_{660}}\\
&b_{28} = \frac{c_{180}c_{210} - c_{280}c_{110}}{\Delta},\ \ \Delta = c_{110}c_{220} - c_{120}c_{210},\\
&b_{32} = -\frac{2c_{661}}{c_{660}},\ \ b_{35} = \frac{c_{350}}{c_{660}}, b_{38} = \frac{c_{380}}{c_{660}},\\
&c_{11i_1} = \int_{-h/2}^{h/2} Q_{11}(\overline{x}_3)x_3^{i_1}\mathrm{d}x_3,\ \ c_{12i_1} = \int_{-h/2}^{h/2} Q_{12}(\overline{x}_3)x_3^{i_1}\mathrm{d}x_3,\\
&c_{21i_1} = \int_{-h/2}^{h/2} Q_{21}(\overline{x}_3)x_3^{i_1}\mathrm{d}x_3,\\
&c_{22i_1} = \int_{-h/2}^{h/2} Q_{22}(\overline{x}_3)x_3^{i_1}\mathrm{d}x_3,\ \ c_{66i_1} = \int_{-h/2}^{h/2} Q_{66}(\overline{x}_3)x_3^{i_1}\mathrm{d}x_3,\ \ i_1 = 0,\ 1,\ 2;\\
&c_{15i_2} = \int_{-h/2}^{h/2} \Gamma_1(x_3)Q_{11}(\overline{x}_3)x_3^{i_2}\mathrm{d}x_3,\ \ c_{18i_2} = \int_{-h/2}^{h/2} \Gamma_2(x_3)Q_{12}(\overline{x}_3)x_3^{i_2}\mathrm{d}x_3,\\
&c_{25i_2} = \int_{-h/2}^{h/2} \Gamma_1(x_3)Q_{21}(\overline{x}_3)x_3^{i_2}\mathrm{d}x_3,\ \ c_{28i_2} = \int_{-h/2}^{h/2} \Gamma_2(x_3)Q_{22}(\overline{x}_3)x_3^{i_2}\mathrm{d}x_3,\\
&c_{35i_2} = \int_{-h/2}^{h/2} \Gamma_1(x_3)Q_{66}(\overline{x}_3)x_3^{i_2}\mathrm{d}x_3,\ \ c_{38i_2} = \int_{-h/2}^{h/2} \Gamma_2(x_3)Q_{66}(\overline{x}_3)x_3^{i_2}\mathrm{d}x_3,\ \ i_2 = 0,\ 1.
\end{aligned}
\tag{A.2}
$$

Appendix B

$$
\begin{aligned}
&s_{11}=\alpha_1^2\left\{\bar{k}_3\left[(a_{11}-a_{31})\alpha_2^2+a_{12}\alpha_1^2\right]-a_{13}\alpha_1^2-\left(a_{14}+a_{32}\right)\alpha_2^2\right\},\\
&s_{11}^{NL}=-\frac{64\bar{k}_1 a_{12}}{3L_1L_2}\frac{\alpha_1^3}{\alpha_1}\left[1-(-1)^m-(-1)^n+(-1)^{m+n}\right],\ s_{11}^{t}=-d_1\alpha_1^2,\\
&s_{12}=\alpha_1\left(a_{15}\alpha_1^2+a_{35}\alpha_2^2+\Gamma_3\right),\ \ s_{12}^{t}=d_2\alpha_1,\ \ s_{13}=(a_{18}+a_{38})\alpha_1^2\alpha_2,\\
&s_{21}=\alpha_2^2\left\{\bar{k}_3\left[a_{21}\alpha_2^2+(a_{22}-a_{31})\alpha_1^2\right]-\left(a_{32}+a_{23}\right)\alpha_1^2-a_{24}\alpha_2^2\right\},\\
&s_{21}^{NL}=-\frac{64\bar{k}_2 a_{21}}{3L_1L_2}\frac{\alpha_2^3}{\alpha_1}\left[1-(-1)^m-(-1)^n+(-1)^{m+n}\right],\ \ s_{21}^{t}=-d_1\alpha_2^2,\\
&s_{22}=(a_{25}+a_{35})\alpha_1\alpha_2^2,\ \ s_{23}=\alpha_2\left(a_{28}\alpha_2^2+a_{38}\alpha_1^2+\Gamma_4\right),\ \ s_{23}^{t}=d_3\alpha_2,\\
&s_{31}=\bar{k}_3\left(\frac{\alpha_1^2}{R_2}+\frac{\alpha_2^2}{R_1}\right),\ \ s_{32}=2\alpha_1^2\alpha_2^2\left(\bar{k}_1+\bar{k}_2\right),\\
&s_{31}^{NL}=-\frac{8}{3L_1L_2}\left[2\left(\frac{\bar{k}_1}{R_2}\frac{\alpha_1}{\alpha_2}+\frac{\bar{k}_2}{R_1}\frac{\alpha_2}{\alpha_1}\right)+\alpha_1\alpha_2\bar{k}_3\right]\\
&\qquad\left[1-(-1)^m-(-1)^n+(-1)^{m+n}\right],\\
&s_{33}=\Gamma_3\alpha_1,\ \ s_{34}=\Gamma_4\alpha_2.
\end{aligned}
\tag{B.1}
$$

where

$$
\bar{k}_1=\frac{1}{32b_{22}}\frac{\alpha_2^2}{\alpha_1^2},\ \bar{k}_2=\frac{1}{32b_{11}}\frac{\alpha_1^2}{\alpha_2^2},\ \bar{k}_3=\frac{\chi_1}{b_{11}\alpha_1^4+(b_{12}+b_{21}+b_{31})\alpha_1^2\alpha_2^2+b_{22}\alpha_2^4}
\tag{B.2}
$$

References

[1] S. Iijima, P. Ajayan, T. Ichihashi, Growth model for carbon nanotubes, Phys. Rev. Lett. 69 (21) (1992) 3100–3103.

[2] M. Meo, M. Rossi, Prediction of Young's modulus of single wall carbon nanotubes bymolecular-mechanics based finite element modelling, Compos. Sci. Technol. 66 (11 and 12) (2006) 1597–1605.

[3] K. Winey, R. Vaia, Polymer nanocomposites, MRS Bull. 32 (4) (2007) 314–319.

[4] N. Fantuzzi, M. Bacciocchi, J. Agnelli, D. Benedetti, Three-phase homogenization procedure for woven fabric composites reinforced by carbon nanotubes in thermal environment, Compos. Struct. 254 (2020) 112840.

[5] O. Gohardanı, M.C. Elola, C. Elızetxea, Potential and prospective implementation of carbon nanotubes on next generation aircraft and space vehicles: a review of current and expected applications in aerospace sciences, Prog. Aerosp. Sci. 3 (2014) 42–68.

[6] A.S. Volmir, The nonlinear dynamics of plates and shells [in Russian], 1972, Moscow: Nauka.

[7] S.A. Ambartsumyan, General theory of anisotropic shells [in Russian], 1974, Moscow: Nauka.

[8] A.H. Nayfeh, D.T. Mook, Nonlinear Oscillations, Wiley, New York, 1979.

[9] M. Amabili, Nonlinear Vibrations and Stability of Shells and Plates, Cambridge University Press, New York, 2008.

[10] K. Yasuda, G. Kushida, Nonlinear forced-oscillations of a shallow spherical-shell, Bul. JSME-Japan Soc. Mech. Eng. 27 (232) (1984) 2233–2240.

[11] M. Amabili, F. Pellicano, M.P. Paıdoussis, Non-linear dynamic and stability of circular cylindrical shells containing flowing fluid, part II: Large-amplitude vibration without flow, J. Sound Vib. 228 (1999) 1103–1124.

[12] M. Amabili, Comparison of shell theories for large amplitude vibrations of circular cylindrical shells: Lagrangian approach, J. Sound Vib. 264 (5) (2003) 1091–1125.

[13] M. Amabili, M.P. Païdoussis, Review of studies on geometrically nonlinear vibrations and dynamics of circular cylindrical shells and panels, with and without fluid-structure interaction, Appl. Mech. Rev. 56 (4) (2003) 349–381.

[14] M. Amabili, Non-linear vibrations of doubly curved shallow shells, Int. J. Nonlin. Mech. 40 (2005) 683–710.

[15] F. Alijani, M. Amabili, K. Karagiozis, F. Bakhtiari-Nejad, Nonlinear vibrations of functionally graded doubly curved shallow shells, J. Sound Vib. 330 (7) (2011) 1432–1454.

[16] F. Pang, H. Li, K. Choe, D. Shi, K. Kim, Free and forced vibration analysis of airtight cylindrical vessels with doubly curved shells of revolution by using Jacobi-Ritz method, Shock Vib. 2017 (2017) 4538540.

[17] K.V. Avramov, S.E. Malyshev, Periodic, quasi-periodic, and chaotic geometrically nonlinear forced vibrations of a shallow cantilever shell, Acta Mech. 229 (4) (2018) 1579–1595.

[18] G.G. Sheng, X. Wang, The non-linear vibrations of rotating functionally graded cylindrical shells, Nonlin. Dyn. 87 (2017) 1095–1109.

[19] G.G. Sheng, X. Wang, Nonlinear vibrations of FG cylindrical shells subjected to parametric and external excitations, Compos. Struct. 191 (2018) 78–88.

[20] M. Bacciocchi, Buckling analysis of three-phase CNT/polymer/fiber functionally graded orthotropic plates: Influence of the non-uniform distribution of the oriented fibers on the critical load, Eng. Struct. 223 (2020) 111176.

[21] H. Ahmadi, A. Bayat, N.D. Duc, Nonlinear forced vibrations analysis of imperfect stiffened FG doubly curved shallow shell in thermal environment using multiple scales method, Compos. Struct. 256 (2021) 113090.

[22] M. Amabili, P. Balasubramanian, Nonlinear vibrations of truncated conical shells considering multiple internal resonances, Nonlin. Dyn. 100 (1) (2020) 77–93.

[23] Y. Liu, Z. Qin, F. Chu, Nonlinear forced vibrations of FGM sandwich cylindrical shells with porosities on an elastic substrate, Nonlin. Dyn. 104 (2021) 1007–1021.

[24] X. Chen, L. Chen, S. Huang, M. Li, X. Li, Nonlinear forced vibration of in-plane bi-directional functionally graded materials rectangular plate with global and localized geometrical imperfections, Appl. Math. Model. 93 (2021) 443–466.

[25] H.S. Shen, Y. Xiang, Nonlinear vibration of nanotube-reinforced composite cylindrical shells in thermal environments, Comput. Methods Appl. Mech. Engrg. 213 (2012) 196–205.

[26] S. Pouresmaeeli, S. Fazelzadeh, Frequency analysis of doubly curved functionally graded carbon nanotube-reinforced composite panels, Acta Mech. 227 (2016) 2765–2794.

[27] M. Avey, E. Yusufoglu, On the solution of large-amplitude vibration of carbon nanotube-based doubly-curved shallow shells, Math. Methods Appl. Sci. (2020) 1–12, http://dx.doi.org/10.1002/mma.6820.

[28] H.S. Shen, Functionally Graded Materials: Nonlinear Analysis of Plates and Shells, CRC Press, Florida, 2009.

[29] A.H. Sofiyev, Review of research on the vibration and buckling of the FGM conical shells, Compos. Struct. 211 (2019) 301–317.

[30] K.M. Liew, Z. Pan, L.W. Zhang, The recent progress of functionally graded CNT reinforced composites and structures, Sci. China Phys. Mech. Astron. 63 (2020) 234601.

[31] A.H. Sofiyev, M. Avey, N. Kuruoglu, An approach to the solution of nonlinear forced vibration problem of structural systems reinforced with advanced materials in the presence of viscous damping, Mech. Syst. Signal Process. 161 (2021) 107991.

[32] A.H. Sofiyev, Application of the FOSDT to the solution of buckling problem of FGM sandwich conical shells under hydrostatic pressure, Compos. B. Eng. 144 (2018) 56–66.

[33] F. Tornabene, N. Fantuzzi, M. Bacciocchi, On the mechanics of laminated doubly-curved shells subjected to point and line loads, Internat. J. Engrg. Sci. 109 (2017) 288–304.

[34] M. Amabili, A new third-order shear deformation theory with non-linearities in shear for static and dynamic analysis of laminated doubly curved shells, Compos. Struct. 128 (2015) 260–273.